

Enhanced magnon transport through an amorphous magnetic insulatorD. M. Cheshire ¹, J. A. D. Nascimento,¹ V. K. Lazarov ^{1,2} and S. A. Cavill ^{1,*}¹*School of Physics, Engineering and Technology, University of York, York YO10 5DD, United Kingdom*²*The York-JEOL Nanocentre, York Science Park, Heslington, York YO10 5BR, United Kingdom*

(Received 22 April 2023; accepted 3 April 2024; published 23 April 2024)

Conduction of spin currents in disordered insulating antiferromagnets has recently been at the center of scientific debate with both long-range spin transport or no spin transport at all observed experimentally. In this study, ferromagnetic resonance has been used to probe the transmission of ac spin current through thin amorphous yttrium iron garnet (YIG) layers. The spin current is found to be mediated by evanescent spin waves with a penetration length four times larger than that of previous studies of amorphous YIG, even exceeding the spin penetration length of crystalline NiO.

DOI: [10.1103/PhysRevB.109.134432](https://doi.org/10.1103/PhysRevB.109.134432)**I. INTRODUCTION**

The long-distance transport of spin currents has been a key focus in spintronics research in recent years due to the drive towards low power spin-based alternatives to complementary metal oxide semiconductor technologies. While earlier work concentrated on the diffusion of spin carried by mobile charges in metals, contemporary research has targeted the propagation of pure spin currents in magnetic insulators [1] where dissipationless transport of the spin has been predicted [2,3]. In a magnetic insulator, the excitation and propagation of spin waves (magnons) are responsible for the transport of the pure spin current. Magnons can be excited across a broad range of energies, with rf magnetic fields (generated by microwave cavities or waveguides) typically used to excite low-frequency, long-wavelength magnons that can propagate coherently over distances of several millimeters in low damping magnetic materials [4]. However, electrical and thermal excitation methods, such as the spin Hall and spin Seebeck effects [5,6], do not provide phase coherent excitation or frequency selectivity. All frequencies with energies $\leq k_B T$ are excited, including a large percentage of magnons with energies comparable to the thermal energy. These are scattered more readily than low-energy magnons, leading to a mean free path that is orders of magnitude shorter [7] with magnon transport occurring diffusively in the incoherent regime.

One magnetic insulator in particular, yttrium iron garnet (YIG), is considered the most prominent material in this field being widely used in spin transport experiments due to its exceptionally low damping, even in thin films. The seminal work by Cornelissen *et al.* first demonstrated long-range

incoherent spin transport in YIG using a nonlocal lateral device geometry [8].

Although YIG has exceptional properties for use in spin-based devices, antiferromagnetic materials have a number of advantages over ferrimagnetic materials such as YIG. The absence of a net magnetic moment makes devices based on antiferromagnetic (AFM) materials stable and resistant to external fields. Furthermore, antiferromagnets have orders of magnitude higher magnetic resonant frequencies that allow for operation in the terahertz regime [9].

One potential issue with AFM materials is that, until very recently, experimental observations have shown that magnon propagation in them is limited to only a few nanometers. This viewpoint was recently disproven when Lebrun *et al.* demonstrated magnon transport over distances of more than 10 μm in a single crystal of the antiferromagnetic insulator hematite ($\alpha\text{-Fe}_2\text{O}_3$) [10]. Following work on thin film $\alpha\text{-Fe}_2\text{O}_3$ highlighted an important point [11]: magnon transport in antiferromagnets is limited by scattering from AFM domain walls thus requiring high-quality samples with small AFM domain wall densities (large antiferromagnetic domains) for long-range magnon propagation.

More recently the observation of exceptionally long micrometer magnon diffusion lengths in amorphous YIG (a-YIG), where there is no significant long-range structural or ferrimagnetic order ($M \approx 0$), was reported [12]. The use of YIG in its amorphous phase is an attractive prospect as stoichiometric YIG thin film growth is challenging, both in maintaining its oxygen content and requiring high thermal budgets ($>700^\circ\text{C}$) to achieve high crystal quality [13]. YIG deposition on certain substrates can also induce dead layers by ion diffusion [14]; these factors limit the efficacy of YIG in magnonic devices, being expensive to produce on large scales, heat sensitive, and difficult to interface with. Magnetic anisotropies in YIG and gaps in its magnon spectrum [15,16] also limit its useful application. The absence of crystal structure in a-YIG eliminates these limiting factors and provides additional advantages, including easier interfacing and negligible phonon contributions.

*Corresponding author: stuart.cavill@york.ac.uk

Spin transport through disordered magnetic insulators, such as a-YIG, is suggested to be mediated by short-range spin correlations and is highly dependent on the relative size of the correlation length to grain size [15]. As amorphous magnetic oxides are potentially devoid of domain walls, depending on the length scale of competing magnetic interactions, this scattering channel is minimized leading to the possibility for long-range spin transport.

However, similar nonlocal experiments have failed to observe long-range spin transport through a-YIG [17], and ferromagnetic resonance (FMR) spin pumping in Permalloy/a-YIG/Pt trilayers provides a much lower (3.6 nm) “magnon diffusion” length for a-YIG [18]. It is well known that pulsed laser deposition (PLD) preserves the final film stoichiometry more than the sputtering technique so that samples of a-YIG may, in fact, have differing levels of “amorphousness” and Fe cation distributions, which are highly dependent on growth conditions. The growth technique and substrate layer may then affect the a-YIG layer, as previously shown to be the case in bulk samples [19], leading to differences in the reported behavior of the magnon penetration length in a-YIG.

In this paper, we report on the magnon penetration length in YIG (45 nm)/a-YIG (t)/Pt (5 nm) trilayer structures. In-plane vector network analyzer FMR (VNA-FMR) spectroscopy was performed to obtain the Gilbert damping of the YIG in the trilayer, as a function of a-YIG thickness (t) and extract the magnon penetration length. The experimental data shows the relationship between damping and a-YIG thickness (t) is described by exponential decay. Moreover, a much larger magnon penetration length is obtained than in previous spin-pumping studies [18].

II. TRILAYER CHARACTERIZATION

YIG films with thickness of 45 nm were grown on (111) $\text{Gd}_3\text{Ga}_5\text{O}_{12}$ (GGG) substrates by PLD. The deposition was performed in high-purity oxygen (2.5×10^{-3} mbar) for 30 min at room temperature using a frequency quadrupled Nd:YAG (yttrium aluminum garnet) laser (266 nm) with a fluence of approximately 1 J cm^{-2} . Post deposition, the YIG films were annealed at 850°C in atmospheric conditions to crystallize the thin films. Samples grown at room temperature, without the annealing step, were found to be amorphous with a magnetization $M \approx 0 \text{ emu/cc}$ [19]. After the growth of the control samples, trilayer samples were grown as follows. YIG films were grown and annealed using the procedure outlined above. An a-YIG layer of thickness t nm was then deposited in a similar manner by PLD at room temperature. The samples were finally capped with 5 nm of Pt to provide the spin sink layer. FMR spin-pumping measurements were performed to ascertain changes to the magnetic damping as a function of a-YIG thickness. In addition, bilayers of YIG (45 nm)/a-YIG (t) were also grown to obtain the change in the magnetic damping as a function of a-YIG thickness without the Pt layer.

A. Structural

All samples were characterized using x-ray diffraction (XRD) around the (444) reflection to confirm epitaxial crystallization of the YIG on the GGG substrate. As bulk materials,

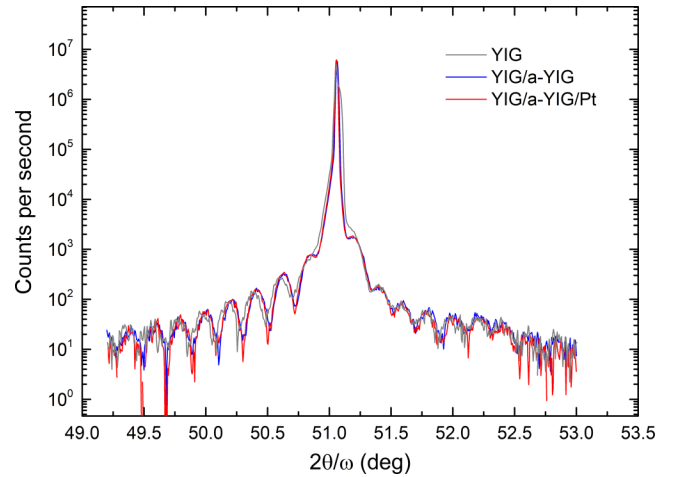


FIG. 1. $2\theta/\omega$ XRD measurement about the (444) reflection for the GGG/YIG (black), GGG/YIG/a-YIG (blue), and GGG/YIG/a-YIG/Pt (red) samples.

the lattice mismatch between YIG and GGG is minimal ($\Delta a = 0.06\%$). As shown in Fig. 1, the corresponding overlap expected between the YIG and GGG Bragg reflections is evidenced by the presence of Pendellösung oscillations close to the GGG(444) reflection. The overlap is so significant that the YIG and GGG peaks cannot be individually separated and adding a-YIG and Pt layers has, within error, no significant effect on the reflection intensity, peak position, nor the period of the fringes showing that the a-YIG layer is amorphous. In addition, a-YIG was grown on the isostructural substrate YAG that, due to its differing lattice constant ($\Delta a = 3.1\%$), allows film and substrate diffraction peaks (if present) to be easily separated. No diffraction peak due to the a-YIG film was observed verifying the amorphous nature of deposited a-YIG layers. X-ray reflectivity (XRR) measurements were also performed to determine the thickness and average roughness of each layer. Figure 2 shows the XRR of the (a) YIG (45) control sample, (b) YIG (45)/a-YIG (21.1) bilayer, and (c) YIG (45)/a-YIG (21.1)/Pt (5) trilayer samples.

The data was fitted using the GENX software package [20]. Refinement protocols based upon a figure of merit (FOM) were used to adjust the parameters to achieve a satisfactory fit using a model as described in [21]. Good agreement is obtained between the model and the experimental data. The generated scattering length density (SLD) plot, Fig. 3(a), shows a sharp interface between each layer demonstrating high-quality films with very limited interdiffusion between layers. For the fitting procedure, fixed densities of 7.08 and 5.17 g cm^{-3} were used for the GGG and YIG, respectively [22]. The a-YIG was modeled with the same parameters as YIG apart from the density, which was allowed to vary from the bulk YIG value. A density slightly less than crystalline YIG was required (5.16 g cm^{-3}) to optimize the FOM. From Fig. 2, a rms roughness of $(0.6 \pm 0.1) \text{ nm}$ was obtained for the a-YIG with a GGG substrate roughness of $(0.7 \pm 0.1) \text{ nm}$. In order to verify the validity of our fitting, cross-sectional transmission electron microscopy (TEM) was performed on the YIG/a-YIG (21.1)/Pt sample as shown in Fig. 3(b). Layer thickness and roughness obtained by cross-sectional TEM

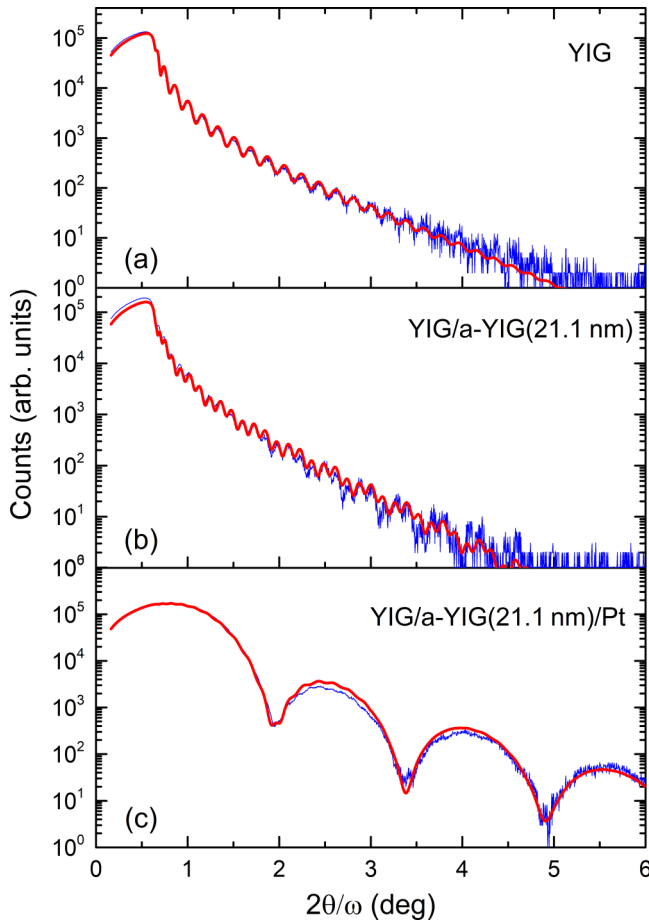


FIG. 2. XRR measurement (blue) with fitted curve (red) for (a) GGG/YIG, (b) GGG/YIG/a-YIG, and (c) GGG/YIG/a-YIG/Pt.

were found to agree, within error, with the parameters extracted from the XRR fitting.

B. Magnetism and FMR spin pumping

Magnetic measurements (M - H loops) were also performed at room temperature by a vibrating sample magnetometer. All samples showed square M - H loops with coercive fields less than 1 Oe, again demonstrating the quality of the crystalline YIG [23]. No increase in the total moment was found after the deposition of a-YIG, even for the thickest a-YIG layer (30 nm), which is comparable to the YIG thickness. Within experimental error (see Supplemental Material), we find no long-range magnetic order of the a-YIG layers, again confirming the amorphous character of the layer.

For the FMR measurements, the sample was mounted face down onto a 50- Ω coplanar waveguide connected to a two-port VNA and centered between the poles of a two-dimensional (2D) vector magnet. Details of the system can be found in [24]. 2D resonance maps were obtained by measuring the s -wave parameter, S_{12} , which is related to the microwave transmission, as a function of frequency and applied field. Field linescans at constant frequency were extracted from the FMR frequency-field maps and fitted using an asymmetric Lorentzian function [25] to determine

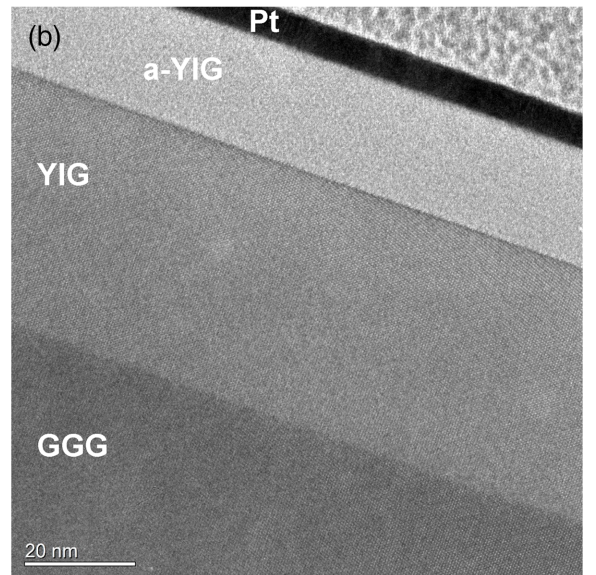
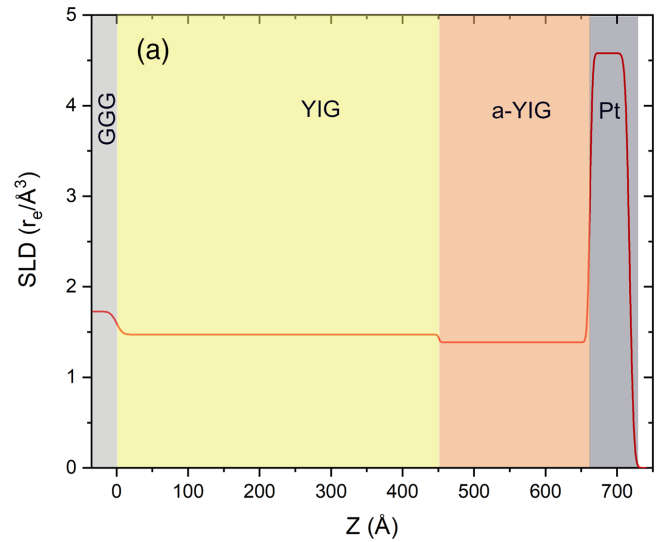


FIG. 3. (a) Scattering length density (SLD) against sample depth (z) simulated from the XRR fitting parameters from Fig. 2(c). (b) Cross-sectional TEM image of the GGG/YIG/a-YIG(21.1 nm)/Pt sample.

the corresponding resonance field (H_r) and linewidth ΔH . The resonance frequency as a function of field is fit to the easy-axis in-plane Kittel equation for a (111)-orientated film, given by

$$\omega = 2\pi\gamma\sqrt{H(H + 4\pi M_{\text{eff}})}, \quad (1)$$

where γ is the gyromagnetic ratio ($\gamma = g\mu_B/\hbar$), M_{eff} the effective magnetization with $4\pi M_{\text{eff}} = 4\pi M_S - \frac{K}{M}$, M_S is the saturation magnetization (136 ± 5 emu/cc) and K is the cubic magnetocrystalline anisotropy constant (-6100 erg/cc for YIG) [26]. M_S determined from the Kittel curve fit agrees within error with independent measurements of the sample using vibrating sample magnetometry [27].

Fits to the data provide a g factor of 1.98 ± 0.01 for all samples, close to the expected value of 2 for a d^5 ion [28]. Slight differences may arise from hybridization of the

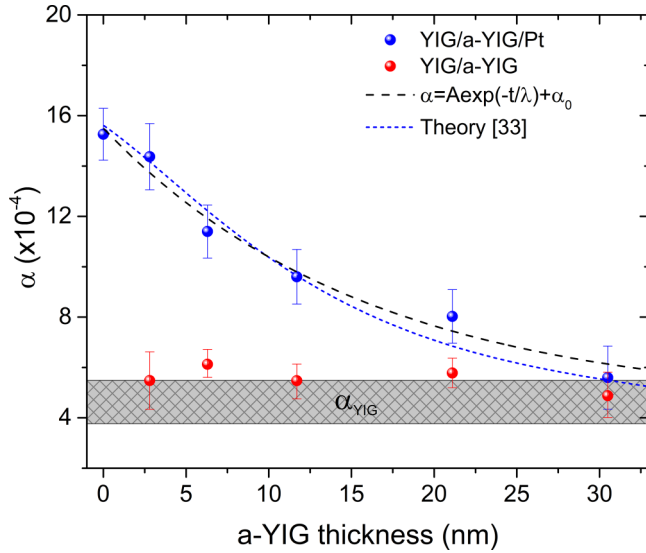


FIG. 4. Extracted Gilbert damping as a function of a-YIG thickness for YIG/a-YIG bilayer (red) and YIG/a-YIG/Pt trilayer (blue). The dashed lines are fits to the data assuming a single (black) or pair (blue) of evanescent modes.

Fe cations with the ligands or a minor underestimate of the experimental uncertainty.

For high-quality samples, where two-magnon scattering is negligible, the field swept linewidth ΔH is linearly dependent on the microwave angular frequency consistent with Gilbert damping such that [23]

$$\Delta H(f) = \Delta H_0 + \frac{2\pi f \alpha}{\gamma}, \quad (2)$$

where ΔH_0 is the frequency independent extrinsic damping. According to spin-pumping theory [29], the spin current sunk by an adjacent layer to the YIG leads to an increase in the Gilbert damping such that $\alpha = \alpha_{\text{intrinsic}} + \alpha_{\text{sp}}$,

$$\alpha_{\text{sp}} = \frac{g\mu_B}{4\pi M_s} g_{\text{eff}}^{\uparrow\downarrow} \frac{1}{d}, \quad (3)$$

where M_s is the saturation magnetization of the YIG, d the YIG layer thickness, and $g_{\text{eff}}^{\uparrow\downarrow}$ is the effective spin-mixing conductance.

The experimental data for magnetic linewidth (ΔH) as a function of microwave frequency can be found in the Supplemental Materials for all samples. Fitting Eq. (2) to the data allows for the extraction of the Gilbert damping (α) and frequency independent extrinsic damping (ΔH_0) as a function of a-YIG thickness. ΔH vs f is linear for all samples indicating that two-magnon scattering is not significant in our samples [21].

Similar to [18], we find a slight change in the extrinsic damping with the deposition of a-YIG on YIG [23], possibly due to a slight increase in roughness of the YIG film at the a-YIG/YIG interface. However, the change in extrinsic damping is not correlated to the a-YIG thickness.

Figure 4 shows the measured α for the trilayer and bilayer samples as a function of a-YIG thickness, t . The bilayer samples show no or very little change in α as a function of a-YIG thickness with α within error of the range

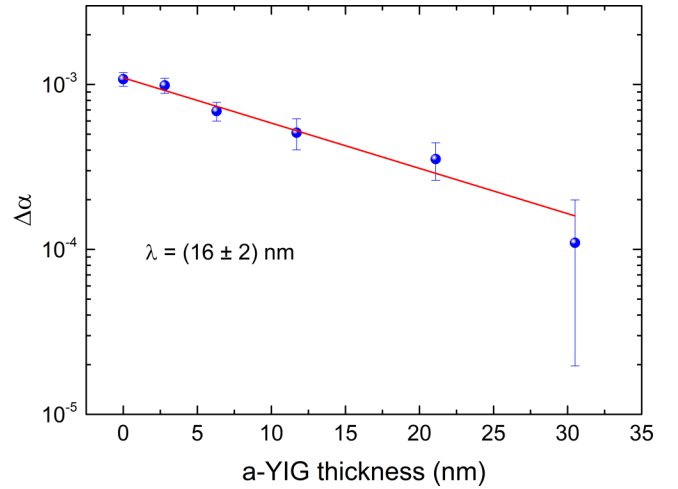


FIG. 5. Spin-pumping contribution to the Gilbert damping as a function of a-YIG thickness (blue data points) fitted with a simple exponential decay with 16 nm characteristic length.

of damping obtained from the single-layer YIG, $\alpha_{\text{intrinsic}} = (4.6 \pm 0.8) \times 10^{-4}$ shown as the gray hashed area in Fig. 4. This is in stark contrast to the results of [18], which show that the Gilbert damping of a YIG/a-YIG bilayer increases significantly (>60%) compared to a single YIG film. The consequence of our result is twofold: either (i) the spins are fully reflected at the interface of the YIG/a-YIG or (ii) the spin waves enter the a-YIG and propagate without being significantly “spin sunk.” The latter description is similar to that of thin Cu layers on a ferromagnetic metal where the Cu thickness is less than the spin diffusion length [30]. To determine which of the scenarios is accurate we performed the same measurements on the trilayer samples.

With the addition of Pt, the damping increases from $\approx 4.6 \times 10^{-4}$ to $\approx 16 \times 10^{-4}$ when no a-YIG is present (i.e., $t = 0$ nm) as expected for spin pumping into a metal with strong spin-orbit coupling [31]. Using Eq. (3) we obtain an effective spin-mixing conductance of $(4.4 \pm 0.5) \times 10^{18} \text{ m}^{-2}$, in close agreement with other studies of YIG/Pt interfaces [32]. As can be seen from Fig. 4, the addition of the a-YIG layer reduces the increase in damping due to spin pumping from the YIG into the Pt. However, with a 10 nm layer of a-YIG there is still a sizable increase in the Gilbert damping due to the spin-pumping effect into the Pt compared to bare YIG or the a-YIG/YIG bilayer. In our samples the spin current is clearly reaching the a-YIG/Pt interface where it is sunk, modifying the YIG α as one would expect from spin-pumping theory [29], and dependent on the a-YIG thickness and propagation length.

Figure 5 shows $\Delta\alpha$ as a function of a-YIG thickness, where $\Delta\alpha = \alpha_{\text{sp}}$. From the linear trend on the log-linear plot, a magnon penetration length (λ) of (16 ± 2) nm is extracted, which is used to plot a simple exponential decay in Fig. 4 (black dashed line). Significantly, no signature of spin-superfluid transport ($1/t$ dependence) is found; spin transport is consistent with either diffusive behavior or evanescent AFM spin-wave modes as we now discuss.

III. DISCUSSION

The spin current is generated by the precessing magnetization in the YIG layer; both YIG and a-YIG are good insulators and no potential difference is applied across the stack, hence we rule out spin diffusion (spin current) mediated by electrons.

In disordered spin systems, such as a-YIG, strong AFM spin correlations typically lead to very small magnetic susceptibilities and very large saturation fields. In this context, we consider the magnetic interactions in thin film a-YIG to be dominated by (local) AFM exchange and use the framework of spin current conduction in antiferromagnetic insulators developed by Khymyn *et al.* [33] to explain the results in this current study. In [33], the authors consider that the spin current in an antiferromagnetic insulator propagates via the excitation of evanescent AFM spin-wave modes. We view this to be analogous to tunneling “leaky” modes in an optical fiber in which the electric field of a waveguide mode decays through the cladding layer and becomes oscillatory at the cladding-air interface, radiating energy away. If the cladding layer is sufficiently thick, the electric field amplitude decays sufficiently so that radiation loss is negligible. In our spin system, the spin current decays through the a-YIG layer with pumped angular momentum lost only if both the AFM layer thickness is comparable to (or less than) the penetration depth of the evanescent mode *and* the spin is sunk by an adjacent heavy metal layer. Hence, the absence of the Pt layer leads to the spin analogy of a “bound waveguide mode” with no loss of pumped angular momentum from the YIG layer and no resultant increase in the Gilbert damping due to spin pumping with the addition of a-YIG. This is in stark contrast to the results of [18] where the deposition of a-YIG on YIG resulted in a significant increase in the Gilbert damping (α).

Using the AFM pair model of Khymyn *et al.* we relate the spin current, due to spin pumping, to the increase in Gilbert damping of the precessing YIG layer. The blue dashed line in Fig. 4 shows a calculation using Eq. (9) from [33] with parameters given in [34]. The theoretical calculation was scaled using a simple numeric prefactor to match the experimental data at $t = 0$ nm only. The best fit to the experimental data is obtained when the penetration lengths for the two AFM spin waves are set to 21.3 and 7.1 nm, respectively. We note that values for AFM spin-wave resonances and velocities do not exist for a-YIG experimentally or theoretically, so we

cannot compare values of the penetration length, obtained from the fit, to those predicted from theory. However, the evanescent AFM spin-wave mode model provides a reasonable first approximation to spin transport in this complex system. In addition, as stated above, we have fitted the data with a single value for the penetration length. Within error, both models give reasonable agreement with the experimental data and similar values for the average decay length: 16 and 14.2 nm, respectively. We also note that recent experiments have shown that spin currents may propagate in insulating antiferromagnets by coherent evanescent spin waves of gigahertz frequency, rather than propagating magnons of terahertz frequency [35]. Such element-specific and phase-resolved measurements [36] would provide an ideal method for studying the dynamics of spin currents through a-YIG spacer layers in appropriate trilayer structures.

IV. CONCLUSION

In conclusion, we demonstrate a significantly enhanced magnon penetration length (16 nm) through a-YIG compared to previous studies of a-YIG and even exceeding that observed in crystalline NiO [37]. An increase in the Gilbert damping of the precessing YIG layer is only observed with the addition of a strong spin-orbit coupled metal (Pt) on top of the a-YIG layer. The results are consistent with the penetration of evanescent spin waves in the a-YIG and analogous to leaky modes in optical waveguides. We again note that our results are in contrast with those of Wang *et al.* [18], who observe an increase of the YIG α due to an adjacent a-YIG layer and no Pt. Importantly our results reopen the discussion on spin current transport through disordered magnetic insulators; we see different behavior for nominally the same system and suggest that this is a clear indication that a-YIG grown under different conditions, using disparate techniques, results in very different spin transport mechanisms. Future work on characterizing the a-YIG layer (correlation length scales) is essential to elucidate the differences reported in the literature and gaining a deeper understanding of magnon propagation in disordered spin systems.

ACKNOWLEDGMENT

We gratefully acknowledge Dr. J. Barker for useful discussions.

-
- [1] A. V. Chumak, V. I. Vasyuchka, A. A. Serga, and B. Hillebrands, Magnonic spintronics, *Nat. Phys.* **11**, 453 (2015).
 - [2] S. Takei, B. I. Halperin, A. Yacoby, and Y. Tserkovnyak, Superfluid spin transport through antiferromagnetic insulators, *Phys. Rev. B* **90**, 094408 (2014).
 - [3] A. Qaiumzadeh, H. Skarsvåg, C. Holmqvist, and A. Brataas, Spin superfluidity in biaxial antiferromagnetic insulators, *Phys. Rev. Lett.* **118**, 137201 (2017).
 - [4] A. A. Serga, A. V. Chumak, and B. Hillebrands, YIG magnonics, *J. Phys. D: Appl. Phys.* **43**, 264002 (2010).
 - [5] S. Zhang, Spin Hall effect in the presence of spin diffusion, *Phys. Rev. Lett.* **85**, 393 (2000).
 - [6] H. Adachi, K.-I. Uchida, E. Saitoh, and S. Maekawa, Theory of the spin Seebeck effect, *Rep. Prog. Phys.* **76**, 36501 (2013).
 - [7] S. R. Boona and J. P. Heremans, Magnon thermal mean free path in yttrium iron garnet, *Phys. Rev. B* **90**, 064421 (2014).
 - [8] L. J. Cornelissen, J. Liu, R. A. Duine, J. Ben Youssef, and B. J. van Wees, Long-distance transport of magnon spin information in a magnetic insulator at room temperature, *Nat. Phys.* **11**, 1022 (2015).
 - [9] F. Keffer and C. Kittel, Theory of antiferromagnetic resonance, *Phys. Rev.* **85**, 329 (1952).
 - [10] R. Lebrun, A. Ross, S. A. Bender, A. Qaiumzadeh, L. Baldrati, J. Cramer, A. Brataas, R. A. Duine, and M. Kläui, Tunable

- long-distance spin transport in a crystalline antiferromagnetic iron oxide, *Nature (London)* **561**, 222 (2018).
- [11] A. Ross, R. Lebrun, O. Gomonay, D. A. Grave, A. Kay, L. Baldrati, S. Becker, A. Qaiumzadeh, C. Ulloa, G. Jakob *et al.*, Propagation length of antiferromagnetic magnons governed by domain configurations, *Nano Lett.* **20**, 306 (2020).
- [12] D. Wesenberg, T. Liu, D. Balzar, M. Wu, and B. L. Zink, Long-distance spin transport in a disordered magnetic insulator, *Nat. Phys.* **13**, 987 (2017).
- [13] S. Emori and P. Li, Ferrimagnetic insulators for spintronics: Beyond garnets, *J. Appl. Phys.* **129**, 020901 (2021).
- [14] A. Mitra, O. Cespedes, Q. Ramasse, M. Ali, S. Marmion, M. Ward, R. M. D. Brydson, C. J. Kinane, J. F. K. Cooper, S. Langridge, and B. J. Hickey, Interfacial origin of the magnetisation suppression of thin film yttrium iron garnet, *Sci. Rep.* **7**, 11774 (2017).
- [15] H. Ochoa, R. Zarzuela, and Y. Tserkovnyak, Spin hydrodynamics in amorphous magnets, *Phys. Rev. B* **98**, 054424 (2018).
- [16] A. J. Princep, R. A. Ewings, S. Ward, S. Tóth, C. Dubs, D. Prabhakaran, and A. T. Boothroyd, The full magnon spectrum of yttrium iron garnet, *npj Quantum Mater.* **2**, 63 (2017).
- [17] L. Yang, Y. Gu, L. Chen, K. Zhou, Q. Fu, W. Wang, L. Li, C. Yan, H. Li, L. Liang *et al.*, Absence of spin transport in amorphous YIG evidenced by nonlocal spin transport experiments, *Phys. Rev. B* **104**, 144415 (2021).
- [18] H. Wang, C. Du, P. C. Hammel, and F. Yang, Spin transport in antiferromagnetic insulators mediated by magnetic correlations, *Phys. Rev. B* **91**, 220410(R) (2015).
- [19] E. M. Gyorgy, K. Nassau, M. Eibschutz, J. V. Waszczak, C. A. Wang, and J. C. Shelton, The magnetic properties of amorphous $\text{Y}_3\text{Fe}_5\text{O}_{12}$, *J. Appl. Phys.* **50**, 2883 (1979).
- [20] M. Bjork and G. Andersson, GenX: An extensible x-ray reflectivity refinement program utilizing differential evolution, *J. Appl. Cryst.* **40**, 1174 (2007).
- [21] C. J. Love, B. Kuerbanjiang, A. Kerrigan, S. Yamada, K. Hamaya, G. van der Laan, V. K. Lazarov, and S. A. Cavill, Substrate dependent reduction of Gilbert damping in annealed Heusler alloy thin films grown on group IV semiconductors, *Appl. Phys. Lett.* **119**, 172404 (2021).
- [22] D. Cheshire, P. Bencok, D. Gianolio, G. Cibin, V. K. Lazarov, G. van der Laan, and S. A. Cavill, Absence of spin-mixed states in ferrimagnet yttrium iron garnet, *J. Appl. Phys.* **132**, 103902 (2022).
- [23] See Supplemental Material at <http://link.aps.org/supplemental/10.1103/PhysRevB.109.134432> for nanodiffraction, magnetometry and FMR data. The Supplemental Material also contains Ref. [38].
- [24] B. Kuerbanjiang, C. Love, D. Kepaptsoglou, Z. Nedelkoski, S. Yamada, A. Ghasemi, Q. M. Ramasse, K. Hamaya, S. A. Cavill, and V. K. Lazarov, Effect of annealing on the structure and magnetic properties of $\text{Co}_2\text{FeAl}_{0.5}\text{Si}_{0.5}$ thin films on Ge(111), *J. Alloys Compd.* **748**, 323 (2018).
- [25] D. E. Parkes, L. R. Shelford, P. Wadley, V. Holý, M. Wang, A. T. Hindmarch, G. van der Laan, R. P. Campion, K. W. Edmonds, S. A. Cavill, and A. W. Rushforth, Magnetostrictive thin films for microwave spintronics, *Sci. Rep.* **3**, 2220 (2013).
- [26] P. Hansen, Anisotropy and magnetostriction of gallium-substituted yttrium iron garnet, *J. Appl. Phys.* **45**, 3638 (1974).
- [27] M_s of the crystalline YIG layer, determined by vibrating sample magnetometry, is (136 ± 5) emu/cc, which is within error of the value determined by FMR with a cubic anisotropy constant $K = -6100$ erg/cc.
- [28] C. Love, J. E. Beevers, B. Achinuq, R. Fan, K. Matsuzaki, T. Susaki, V. K. Lazarov, S. S. Dhesi, G. van der Laan, and S. A. Cavill, Anisotropy and magnetostriction of gallium-substituted yttrium iron garnet elucidation of orbital moment, anisotropy, and magnetic damping in epitaxial Fe_3O_4 films, *Phys. Rev. B* **107**, 064414 (2023).
- [29] Y. Tserkovnyak, A. Brataas, and G. E. W. Bauer, Spin pumping and magnetization dynamics in metallic multilayers, *Phys. Rev. B* **66**, 224403 (2002).
- [30] S. Yakata, Y. Ando, T. Miyazaki, and S. Mizukami, Temperature dependences of spin-diffusion lengths of Cu and Ru layers, *Jpn. J. Appl. Phys.* **45**, 3892 (2006).
- [31] S. Mizukami, Y. Ando, and T. Miyazaki, Effect of spin diffusion on Gilbert damping for a very thin permalloy layer in Cu/permalloy/Cu/Pt films, *Phys. Rev. B* **66**, 104413 (2002).
- [32] M. Haertinger, C. H. Back, J. Lotze, M. Weiler, S. Geprägs, H. Huebl, S. T. B. Goennenwein, and G. Woltersdorf, Spin pumping in YIG/Pt bilayers as a function of layer thickness, *Phys. Rev. B* **92**, 054437 (2015).
- [33] R. Khymyn, I. Lisenkov, V. S. Tiberkevich, A. N. Slavin, and B. A. Ivanov, Transformation of spin current by antiferromagnetic insulators, *Phys. Rev. B* **93**, 224421 (2016).
- [34] Following Eq. (9) in [33], we use $\beta = 1$, $\lambda_1 = 21.3$ nm, $\lambda_2 = 7.1$ nm, and a phase shift between the two evanescent waves of $\pi/2 - 0.0005$.
- [35] M. Dabrowski, T. Nakano, D. M. Burn, A. Frisk, D. G. Newman, C. Klewe, Q. Li, M. Yang, P. Shafer, E. Arenholz *et al.*, Coherent transfer of spin angular momentum by evanescent spin waves within antiferromagnetic NiO, *Phys. Rev. Lett.* **124**, 217201 (2020).
- [36] C. J. Durrant, L. R. Shelford, R. A. J. Valkass, R. J. Hicken, A. I. Figueroa, A. A. Baker, G. van der Laan, L. B. Duffy, P. Shafer, C. Klewe *et al.*, Dependence of spin pumping and spin transfer torque upon $\text{Ni}_{81}\text{Fe}_{19}$ thickness in Ta/Ag/ $\text{Ni}_{81}\text{Fe}_{19}$ /Ag/ Co_2MnGe /Ag/Ta spin-valve structures, *Phys. Rev. B* **96**, 144421 (2017).
- [37] H. Wang, C. Du, P. C. Hammel, and F. Yang, Antiferromagnonic spin transport from $\text{Y}_3\text{Fe}_5\text{O}_{12}$ into NiO, *Phys. Rev. Lett.* **113**, 097202 (2014).
- [38] Y. J. Kim, C.-Y. Liu, S. K. Lamoreaux, G. Visser, B. Kunkler, A. N. Matlashov, J. C. Long, and T. G. Reddy, New experimental limit on the electric dipole moment of the electron in a paramagnetic insulator, *Phys. Rev. D* **91**, 102004 (2015).